JOURNAL OF GEOPHYSICAL RESEARCH, VOL. 112, D18103, doi:10.1029/2007JD008451, 2007



# Ob' River flood inundations from satellite observations: A relationship with winter snow parameters and river runoff

F. Papa,[1,2] C. Prigent,[3] and W. B. Rossow[2]

Received 23 January 2007; revised 15 May 2007; accepted 20 June 2007; published 19 September 2007.

[1] Using a multisatellite method, including passive microwave land surface emissivities, along with active microwave, visible and near infrared observations developed to estimate global inundated area, we examine the spatial and temporal variations of the 1993–2000 monthly inundation extents over a Boreal environment, the Ob River basin. Over the entire watershed, the mean extent of inundation during the snow-free months is $2.6 \times 10^5$ km$^2$, consistent with previous independent static or satellites-derived estimates. The maximum in yearly inundation, showing propagation from south to north between April and June, exhibits strong seasonal and inter-annual variations. The consistency of the inundation estimates is then analyzed at local or basin-wide scale using different in situ or satellite-derived snow and runoff parameters. The results show a strong relationship between the inundation extent and the snowmelt date, the snowpack depth at three in situ stations located in the southern part of the basin. Over the northern part, results show that flooding is more closely linked to the amount of water coming downstream from the southern part of the basin. A close systematic relationship is also found between the inundation extent and the local in situ runoff at six locations as well as with the altimeter-derived discharge measured at the Ob estuary. This case study evaluation shows the potential of these data sets to provide consistent information about the seasonal and inter-annual variations of inundation over a major Boreal river basin. These results also suggest new potential to improve the description of the snow-inundation-runoff relationship that are fundamental for climate and hydrological models.

**Citation:** Papa, F., C. Prigent, and W. B. Rossow (2007), Ob' River flood inundations from satellite observations: A relationship with winter snow parameters and river runoff, *J. Geophys. Res.*, *112*, D18103, doi:10.1029/2007JD008451.

## 1. Introduction

[2] Wetlands and episodically flooded areas are an integral part of the biochemical and the hydrological cycles. They are the world's dominant natural source of methane (CH4) and the only one dominated by short-term climate variations. They account for ~40% of the methane emission annually into the atmosphere [*Matthews*, 2000] and the fluctuations in wetlands and inundation extents appear to be the major contributors to interannual variability in methane surface emissions [*Bousquet et al.*, 2006]. About 30% of methane emission comes from the high northern latitudes [*Walter et al.*, 2001], the Ob River in Russia representing one of the boreal hot spots [*Houweling et al.*, 1999]. Wetlands and inundated surfaces also play a key role in local hydrological systems. They regulate river hydrology and process a part of the fresh water input by rivers to oceans. In high latitudes, quantifying the part of the fresh water input into the northern oceans by river discharge is crucial as it greatly influences the Arctic Ocean freshwater budget, the thermoaline circulation and the winter sea ice cover [*Dickinson et al.*, 2001]. With the largest watershed of all Artic rivers (~3 millions km$^2$), the Ob River in Russia is the third largest freshwater contributor of the Eurasian rivers to the Artic Ocean after the Yenisey and the Lena Rivers.

[3] Flooded areas and the rivers may also be indicators of climate change. The average annual discharge of fresh water from the six largest Eurasian rivers to the Artic Ocean has increased by 7% over the last century [*Peterson et al.*, 2002].

[4] Approximately 60% of the world wetlands are inundated only during some portion of the year, leading to large seasonal and interannual variability of their extents. This is particularly true for the Northern latitudes and the Ob river basin which are influenced by the winter snow and freeze/thaw cycles leading to extreme flooding events during the spring/summer season [*Yang et al.*, 2003]. The winter water storage as snow and its subsequent release upon melting are one of the major factors that influence the northern latitude river discharge [*Cao et al.*, 2002; *Yang et al.*, 2003]. Recently, warmer air temperatures in May have been related to an increase in snowmelt runoff and associated extremely large floods events for the Lena River [*Yang et al.*, 2002].

[1] NASA-Goddard Institute for Space Studies-Columbia University, New York, USA.
[2] NOAA-Cooperative Remote Sensing Science and Technology Center, City College of New York, New York, USA.
[3] CNRS, Laboratoire d'Etudes du Rayonnement et de la Matiere en Astrophysique, Observatoire de Paris, France.


0148-0227/07/2007JD008451$09.00

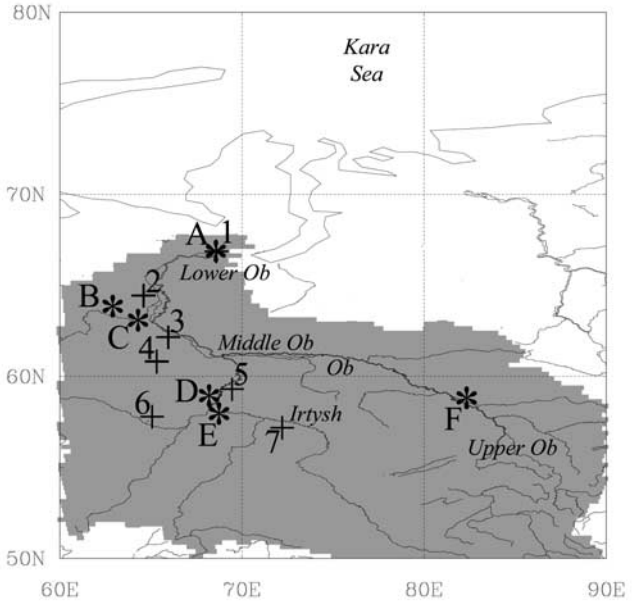


**Figure 1.** The Ob watershed and the in situ stations network. The locations of the 7 stations related to snow in situ measurements are displayed with cross (+) and referenced with numbers. The six in situ river runoff gauging-stations are displayed with star (*) and referenced with letters.

[5] Thus reliable and timely information about the extent, spatial distribution and temporal variation of wetlands and floods is crucial to better understand their relationships with winter snow properties and river discharges, as well as their influence on regional hydrology and climate.

[6] Existing global data sets are generally static inventories and are defined mainly by ecology and soil classification [*Matthews*, 2000]. Satellite-derived inundation extents and their dynamics are being actively investigated [*Smith*, 1997; *Mialon et al.*, 2005; *Papa et al.*, 2006a] as they provide a unique means to observe continuously large regions and are the only alternative to the lack of in situ data in remote areas. A globally applicable Remote Sensing (RS) technique, using a suite of complementary satellite observations, has been developed to quantify the spatial and temporal dynamics of wetlands and inundation [*Prigent et al.*, 2001a; *Prigent et al.*, 2007]. It is based on the detection of water surfaces using passive microwave land surface emissivities estimated from SSM/I observations, along with ERS scatterometer and AVHRR visible and near infrared reflectances to estimate the vegetation contribution to the passive microwave signal [*Prigent et al.*, 2001a, 2007; *Papa et al.*, 2006b]. Global monthly mean estimates of inundation extent are now available for the period 1993–2000 [*Prigent et al.*, 2007].

[7] For most areas, and particularly in Northern Eurasia, the performance of the above method in estimating the seasonal and interannual variability of inundation has not been fully evaluated due to the scarcity of in situ measurements to compare with. This multisatellite method has been carefully evaluated over the Indian Subcontinent [*Papa et al.*, 2006b] and over other tropical or sub-tropical environments such as the Amazon River and major African or Asian River basins [*Prigent et al.*, 2007]. This study extends the evaluation of these estimates into a different regime, a boreal river basin.

[8] We assess the seasonal and the interannual variability of the satellite-derived inundation extents for the Ob River basin over the 1993-2000 period using different proxies. First, we investigate the relation of inundation extent to winter snow parameters (snow depth and snowmelt date) obtained from in situ measurements at seven different stations located in the Ob river basin as well as the snow estimates derived from passive microwave remote sensing data. Then, the in situ monthly run-off observations at six different locations along the rivers, including a station at the Ob estuary, as well as satellite radar altimeter-derived discharges, are compared with inundation extent variations. There are two objectives: (a) verify the annual and interannual variations of the multisatellite derived inundations and (b) understand better the relations among inundation extents, the snowpack characteristics and the river runoff at the local scale and over this large boreal river basin.

## 2. Study Area and Data

### 2.1. The Ob River

[9] The Ob basin has the largest watershed of all Artic rivers (2,975,106 $km^2$) with a mean annual flow of 402 $km^3/s$ and is one of largest contributors of fresh water to the Artic Ocean. The Ob originates in the Altai Mountains and flows northward across a vast West Siberian lowland toward the Arctic Ocean. A large part of the Ob watershed is located within the Western Siberian plain characterized during the spring-summer seasons by large flooded areas frequently described as the world's biggest swamp. The Ob river length is 3680 km and with its major tributary, the Irtysh, it forms the longest river system in Asia. The watershed is usually divided into three main parts as indicated on Figure 1: the upper Ob, the middle Ob-Irtysh rivers region and the lower Ob [*Kouraev et al.*, 2005]. The absence of topographic relief significantly affects the hydrographic network, which exhibits a sharp asymmetry with 67% of the watershed located on the left bank. Another notable feature is the presence of areas of inner discharge in the upper Ob region, between the Ob and the Irtysh. Although a part of the Ob watershed, these areas, which covers 15% of the total basin, do not provide inflow to the Ob river system. In the region of the Irtysh-Lower Ob, there are 70,000 water streams, 89% are less than 10km long, and over 450,000 small lakes with a surface area less than 1 $km^2$.

[10] During the winter, the majority of the basin is covered by snow, which persists for six months or more. The latitudinal extent of the Ob basin results in the gradual snowmelting from south to north during spring. Snowmelt typically begins in April in the southern reaches of the basin but does not occur until June near the mouth of the Ob. The distribution of the river discharge in various part of the Ob river system has complex patterns with long flooding periods. The Ob discharge starts increasing in April and the maximum flow usually occurs in May-June when the south-north flood wave finally begins to break the ice cover. During this time, large areas of the Ob basin are flooded.

**Table 1.** In Situ Snow Parameters: Station Names and Coordinates, the Mean and the Associated Standard Deviation at Each Site for the Snow Depth (SD) for January–February–March–April 1993–1996, the Maximum Snow Depth for 1993–1996, the Snow Depth in February 1993–1996 and the Snowmelt Date[a]

| | SD JFMA, cm | | SD Max., cm | | SD February, cm | | Snowmelt Date, day | |
|---|---|---|---|---|---|---|---|---|
| Station | Mean | Std | Mean | Std | Mean | Std | Mean | Std |
| 1-Shalekard 66.32°N–66.32°E | 35.00 | 9.55 | 43.13 | 6.02 | 41.70 | 8.15 | 126 | 15 |
| 2- Berezevo 63.56°N–65.03°E | 53.91 | 17.07 | 63.80 | 16.17 | 57.80 | 18.16 | 126 | 15 |
| 3-Oktjarbrskoe 62.27°N–66.03°E | 71.63 | 20.26 | 84.72 | 16.05 | 77.90 | 14.01 | 124 | 14 |
| 4-Saim 60.19°N–64.13°E | 28.71 | 14.74 | 40.88 | 4.89 | 40.88 | 4.89 | 110 | 16 |
| 5-Demjamskoe 59.36°N–69.17°E | 52.40 | 17.23 | 65.22 | 7.10 | 63.15 | 10.55 | 109 | 11 |
| 6-Turinsk 58.03°N–65.21°E | 35.20 | 16.95 | 49.70 | 8.64 | 49.05 | 9.59 | 102 | 10 |
| 7-Ustisim 57.43°N–71.11°E | 53.22 | 20.06 | 69.05 | 9.94 | 64.62 | 10.66 | 108 | 14 |

[a]The stations are located on Figure 1.

[11] The only large reservoir on the Ob is located near Novosibirsk, at the southeastern end of the basin, but this diversion is rather small and has little impact on the total flow entering the Arctic Ocean.

[12] We will consider the values of parameters spatially averaged over the Ob River Basin (ORB) which ranges from (52N–68N/61E–91E).

### 2.2. Satellite Derived Inundation Extent

[13] The methodology developed to quantify the extent and seasonality of land inundation at global scale with a suite of satellites is described in detail by *Prigent et al.* [2001a, 2007]. The selected satellite observations used to detect and quantify inundation cover a large wavelength range:

[14] (a) passive microwave emissivities at 37 GHz (0.81 cm), estimated from SSM/I by removing the contributions of the atmosphere (water vapor, clouds, rain) and the modulation by the surface temperature, using ancillary data from visible and infra-red satellite observations from the International Satellite Cloud Climatology Project (ISCCP) [*Rossow and Schiffer*, 1999] and the National Center for Environment Prediction (NCEP) reanalysis [*Kalnay et al.*, 1996]

[15] (b) ERS-1 scatterometer (active microwave) backscatter at 5.25 GHz (5.71 cm);

[16] (c) AVHRR Normalized Difference Index Vegetation NDVI.

[17] A full description of each satellite observation and the potential of merged satellite data to study wetlands and inundated surfaces can be found in *Prigent et al.* [2001b]. The complete methodology developed to quantify water surfaces extent and dynamic on the global scale is illustrated by *Prigent et al.* [2007] and over a specific region such as India by *Papa et al.* [2006b].

[18] The data set can be summarized as follows. All remote sensing data are averaged over each month at an equal area interval of 0.25° at the equator (a pixel equals to 773 $km^2$) for the period 1993-2000. The methodology used to estimate monthly flooded areas is then based on the estimation of pixel fractional coverage by open water using the passive microwave signal and a linear mixture model with end-members calibrated for each location with radar observations to account for the effects of vegetation cover [*Prigent et al.*, 2001a].

[19] As the microwave measurements are also sensitive to the snow cover, the snow and ice mask from the NSIDC [*Armstrong and Brodzik*, 2005] has been used to edit the results and avoid any confusion between snow cover and snow-free pixels. The weekly North Hemisphere snow mask given by NSIDC at 25 km interval comes from AVHRR, GOES, and other visible-band satellite data.

[20] Global monthly mean maps of inundation extent are then created for the period 1993-2000. The technique is globally applicable without any tuning for individual environments [*Prigent et al.*, 2007].

[21] In this study, four other data sets are used to check the consistency of the satellite-derived inundation extent and variations: 1) the local snow depth and the snowmelt date from in situ observations at seven different locations, 2) the snow depth derived from SSM/I measurements over the Ob River Basin 3) the Ob River runoff from in situ data at six locations, 4) the Ob River discharge estimated from a satellite altimeter at the estuary. These data sets offer a reliable time evolution to compare with. The independent nature of each data set is meantionned in the following sections.

### 2.3. Snow Data Sets

#### 2.3.1. In Situ Snow Data Set

[22] The first snow data set is issued from the Former Soviet Union Hydrological Snow Survey based on in situ observations [*Krenke*, 2004]. Among the 1345 sites throughout the Former Soviet Union, most of them have observations until 1990 but only 238 of those sites have updated measurements through 1996. As the satellite-derived inundation product covers the period 1993-2000, coincident observations from only seven stations are available over the Ob. The locations of these stations are shown by crosses in Figure 1 and the names and coordinates are given in Table 1. For each station, two snow parameters are used: 1) the monthly average snow depth calculated from the ten-day average of individual snow depth measurements at each station; 2) the snowmelt date deduced from the number of days of snow presence in a month at each station (with a precision of 5 days). The snow parameter characteristics for each individual station are summarized in Table 1. The in situ snow data set and the inundation extent data set are fully independent information.

#### 2.3.2. Satellite Derived Snow Data Set

[23] The second snow data set is derived from passive microwave observations from SSM/I and a specific methodology explained by *Grippa et al.*, 2005. Two snow parameters are obtained: 1) the timing of snowmelt, obtained when comparing the SSM/I 19 and 37 GHz horizontally polarized channels that detect the presence or

**Table 2.** Descriptions of the Stations and the In Situ Runoff Observations[a]

| Station | River Name | Drainage Area, km$^2$ | Runoff, m$^3$/s | | Data Time Coverage | Topography, m | |
|---|---|---|---|---|---|---|---|
| | | | Mean | Std | | Mean | Std |
| A-Shalekard 66.63°N–66.60°E | Ob | 295,0000 | 13,064.50 | 10,669.90 | 1993–2000 | 193.02 | 84.06 |
| B-Sosva 63.65°N–62.10°E | Severnaya | 87,800 | 690.34 | 942.12 | 1993–1999 | 178.54 | 60.96 |
| C-Igrim 63.18°N–68–80°E | Severnaya | 87,800 | 904.12 | 1034.45 | 1993–1999 | 112.24 | 15.57 |
| D-Bolchary 59.82°N–68.80°E | Konda | 65,400 | 427.81 | 246.75 | 1993–1998 | 75.95 | 7.39 |
| E-Tobolsk 58.20°N–68.23°E | Irtysh | 1,500,000 | 2393.98 | 1811.23 | 1993–1999 | 65.62 | 11.26 |
| F-Kolpachevo 58.30°N–82.88°E | Ob | 2,950,000 | 3318.68 | 2887.17 | 1993–1994<br>1997–1999 | 95.93 | 8.09 |

[a]The stations providing the in-situ runoff are located with stars on Figure 1.

absence of snow on the ground and 2) the snow depth, estimated by using a dynamic algorithm mixing SSM/I brightness temperatures at 19 and 37 GHz and a model from the thermal gradient in the snowpack [*Josberger and Mognard*, 2002]. The snow depth estimates used here are obtained through a specific method recently adapted to the Siberian regions [*Grippa et al.*, 2004].

[24] However, as the satellite-derived snow parameters and the satellite-derived inundation are estimated from the same passive microwave sensor, SSM/I, the two data sets are not strictly independent. We do not use the satellite-derived timing of snowmelt. Since the timing of snowmelt and the beginning of the flooding events are closely connected, we check of the consistency of the inundation data set using the snowmelt dates from in situ observations only. However, we do use the SSM/I-based snow depth values (in cm) spatially averaged over the ORB for the month of February [*Grippa et al.*, 2005]. As we found no flooding events in February, these two data sets can be considered as independent.

### 2.4. Runoff and Discharge Data Set

#### 2.4.1. In Situ Runoff

[25] The in situ runoff data (m$^3$/s) are measured at six different stations located along the Ob and the Irtysh Rivers or small-connected rivers. They are the only gauging stations in the region for which appropriate date are available. Monthly mean values are obtained from the R-Artic web site [*R-Artic*, 2003]. The locations of these gauging-stations are shown in Figure 1 with stars and referenced with letters. A key site is the Shalekard station, the last observation point before the Ob enters the Kara Sea situated at (66.63°N–66.60°E). Discharge data collected at the river mouth are particularly important as they represent freshwater input to the ocean and are often used for basin-scale water balance calculations and validation of hydrological modeling.

[26] Table 2 summarizes the runoff data set with the principal characteristics of each station. The topography characteristics in Table 2 are taken from the US Naval topography data set averaged to a 1 × 1 degree resolution. The in situ runoff data set and the inundation extent data set are fully independent.

#### 2.4.2. Satellite Altimeter-Derived Discharge

[27] Originally designed to operate over the ocean, the radar altimeter also provides time series of water-levels for large water bodies (rivers, lakes) thanks to a specific retracking and data analysis procedure [*Fung and Cazenave*, 2001; *Gennero et al.*, 2005]. Using the Topex-Poseidon radar altimeter, *Kouraev et al.* [2005] estimated the Ob River water discharge close to the Shalekard station using the satellite-derived water levels. In the present study, we use the monthly altimeter-derived river discharge estimates covering the 1993-2000 period. According to *Kouraev et al.* [2005], the interannual variability of water discharge is caused by early or late spring flooding but this has not been yet checked against an inundation data set. The satellite-derived runoff data set and the inundation extent data set are fully independent.

[28] Along with the four data sets described previously, we also looked in this study at other components that could play a role in the hydrological processes of the Ob River Basin such as rain distribution and permafrost cover. The Global Precipitations Climatology Product version 2 products (GPCP), which quantify the distribution of precipitation over the whole globe [*Adler et al.*, 2003] were investigated. The Satellite-Gauge Combined Precipitation Data product (monthly means, initial spatial resolution of 2.5° of latitude and longitude but regridded on a 0.25° equal area grid) exhibits a large interannual variability over the Ob River basin with maximum values in July. The average value for the entire basin of monthly precipitation at maximum is 2.1 mm/day. Since precipitation over the Ob basin is not a significant contributor to flooding events, it is not discussed further.

[29] Melting of permafrost might also be considered as a factor that could influence the inundation and the discharge of rivers flowing in northern Siberia. However, for the Ob River, the discontinuous permafrost is only located in a small area in the northern part of the basin, covering only 4%–10% of the entire Ob watershed. [*Zhang et al.*, 1999]. Melting of permafrost is not a significant contribution to flooding and to the total discharge of the Ob River [*Yang et al.*, 2002].

## 3. Flooding in the Ob River Basin

[30] Figure 2 shows the temporal evolution of the total inundated extent (km$^2$) over the Ob River Basin for the period 1993-2000. The mean extent during the snow-free months is $2.6 \times 10^5$ km$^2$. This value accords well with the $2.8 \times 10^5$ km$^2$ estimate of maximum flooding from

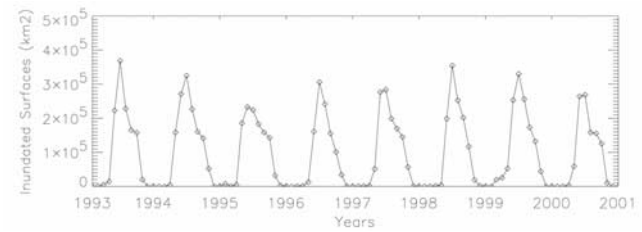


**Figure 2.** Seasonal variations of the inundated areas ($km^2$) over the Ob River Basin (52N–68N/61E–91E) from 1993 to 2001.

*Matthews and Fung*, 1987, for the same area from aeronautical charts. [*Prigent et al.*, 2007] (not shown). The value also accords well with the estimates by *Mialon et al.* [2005] retrieved from SSMI 19 and 37 GHz brightness temperature measurements ($2.2 \times 10^5$ $km^2$) and the estimates derived from radar altimeter backscatters observations ($2.78 \times 10^5$ $km^2$) by *Papa et al.* [2006a].

[31] The inundation show a strong seasonal cycle, with the flooding starting in May and lasting until the end of the summer. It also shows a noticeable interannual variability. In 1993, the maximum inundated extent reached $3.67 \times 10^5$ $km^2$ whereas in 1995, it only reached $2.57 \times 10^5$ $km^2$. The inundation extent always reaches its maximum in June, except for 1995 where the maximum occurred in May.

[32] Figure 3a displays maps of the annual maximum of fractional inundation extent (in %, 100% of inundations equals to an area of 773 $km^2$) from satellite estimates for each year of the period 1993-2000. Figure 3b shows the corresponding month during which the maximum inundation is reached. Figure 3a clearly shows that the geographical structures are well captured for the Ob river system. The two main rivers channels, the Ob and the Irtysh (compare with Figure 1) and the associated inundation areas are well delineated. There is a strong signature with high fractional inundation extent (50–90%) in the region (60°N–66°N/65°E–78°E) where the two rivers meet. These realistic structures are in good agreement with *Matthews and Fung* [1987]'s spatial features (not shown). The results also show low variability in the spatial structure of the annual maximum. However, the values of the total inundated areas at maximum exhibit noticeable inter-annual variability. For the years 1993, 1994, 1998, 1999, Figure 3a shows extremely large flooded areas in the middle Ob and along the downriver stream. This is consistent with the interannual variability of the total inundated extent over the whole basin in Figure 2.

[33] Figure 3b shows the evolution of the date (month) during which maximum inundation extent occurred. It

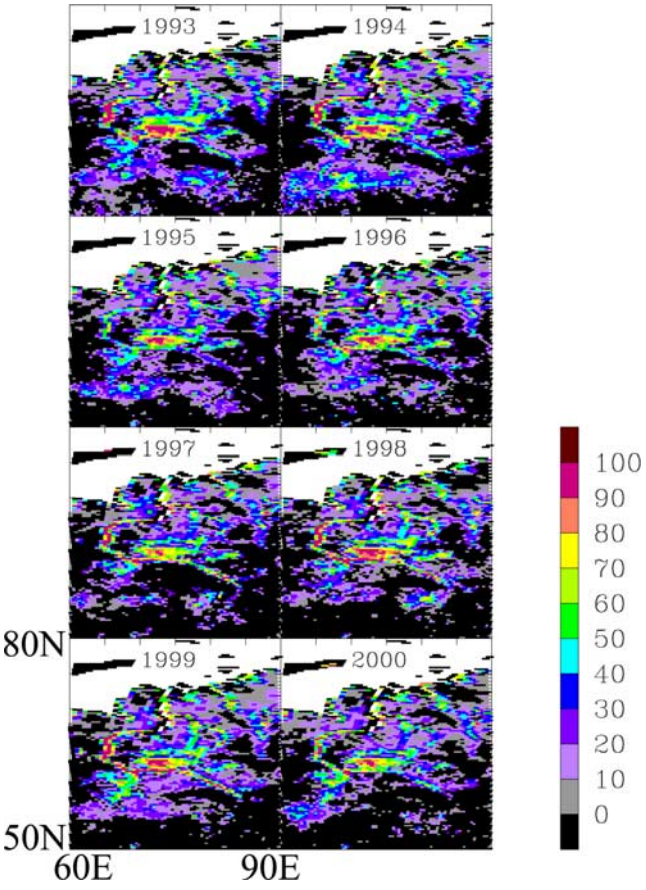


**Figure 3a.** Satellite-derived inundations result over the Ob River Basin for the 1993–2000 period with a 773 $km^2$ spatial resolution: the fractional inundation at maximum for each year (%).

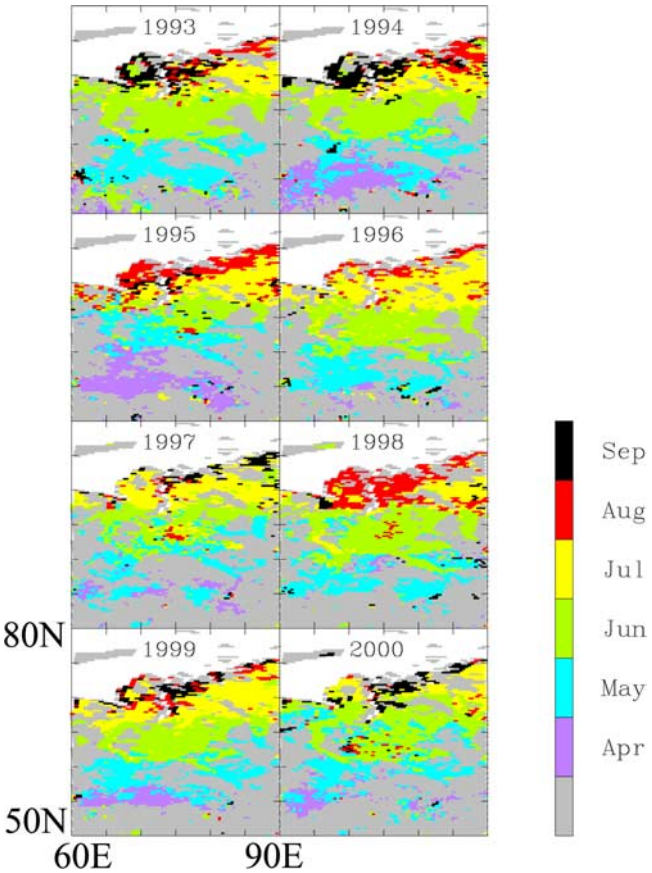


**Figure 3b.** Satellite-derived inundations result over the Ob River Basin for the 1993-2000 period with a 773 $km^2$ spatial resolution: the month where the fractional inundation is maximum for each year.

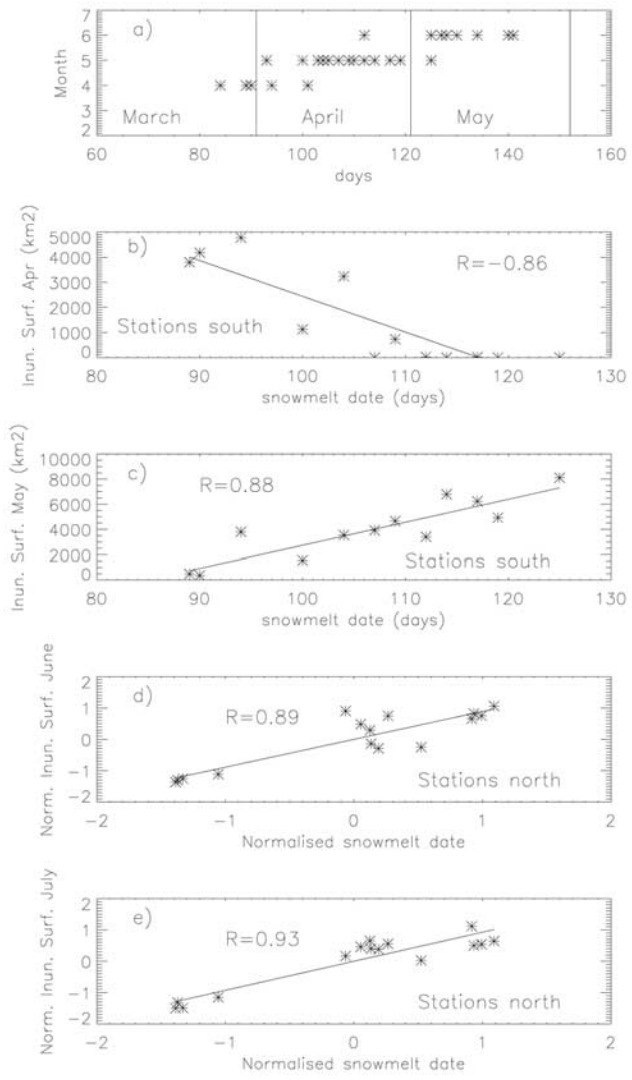


**Figure 4.** Scatterplot and linear regression results of the in situ snowmelt date observations and the satellite-derived inundated surfaces calculated over a $1^\circ \times 1^\circ$ area centered on each station during the 1993–1996 period (a) the snowmelt date versus the month of inundated surfaces at maximum for the 7 stations (b) and (c) the snowmelt date versus the inundated surfaces in April and May for the southern stations (stations 5, 6, 7) (d) and (e) the normalized (the mean is subtracted and the resulting values are divided by the standard deviation over the period) snowmelt date versus the normalized inundated surfaces in June and July for the northern stations (stations 1, 2, 3, 4).

clearly shows a propagation from south to north resulting from the latitudinal dependence of the snow melting. The maximum inundation extent occurs from April to May in the southern part of the Basin and from May to June on the northern region. The propagation of the maximum inundation extent from south to north generally takes three months (this estimate is limited by the monthly temporal resolution of the data set). In the far north (not a part of the Ob river basin), the maximum inundation extent occurs even as late as July–August. Interannual variability is exhibited for instance, by the differences in timing and magnitude observed between 1994 and 1995 in a large part of the lower basin. In 1995 and 1997, the maximum inundation in the middle-upper Ob occurred in May, instead of in June as it did in the other years.

[34] In order to evaluate the consistency of the temporal and spatial evolution of inundation over the Ob River Basin, we look in the following sections at other water balance measurements at the local scale or basin-wide scale.

## 4. Flooding and Snow Relations

### 4.1. Local Study Using In Situ Snow Parameters

[35] A first analysis of the in situ snow parameters shows no evident correlation between the snowmelt dates and the snow depth at any site for the 4 years; a deeper snowpack does not seem to increase the duration of snow cover which confirms that the melting process is mostly driven by the local air temperatures [*Grippa et al.*, 2005].

[36] We compare the variations of the inundation extent at each station, calculated over a $1^\circ \times 1^\circ$ area centered on the coordinates of the station. Figure 4 summarizes the results of the comparison between the satellite-derived inundation extent and the in situ snowmelt date. Figure 5 summarizes the comparison with the in situ snowpack depth.

[37] Figure 4a displays a scatterplot of the in situ snowmelt date for each station for the period 1993-1996 versus the month of maximum inundation extent (28 points). Considering the monthly temporal resolution of the inundations data set, there is a lag of 0 (3 cases), 1 (25 cases) or 2 (1 case) months between the snowmelt date and the month of maximum inundation extent. Although expected, this result shows the consistency of the inundation timing estimates.

[38] Considering now the ensemble of the snow observations (the seven stations over the period 1993–1996) versus the inundation extent (28 points), the results show: (a) a poor linear correlation between the snowmelt date and the inundated extent in May (-0.18) and a low linear correlation between the snowmelt date and the inundated extent in June (0.54); (b) a low linear correlation between the maximum snow depth and the maximum inundated extent (−0.36). For the present case, coefficients with absolute values higher than 0.374 are statistically significant at 95% confidence level (the level of significance of two-tailed test is $P \leq 0.05$). For the ensemble of station measurements over the period 1993–1996, there is no evidence of a clear relation between either the snowmelt date and the inundated extent, or between the snow depth and the inundated extent at maximum.

[39] Now we consider two sub-ensembles of the stations: a) the southern stations (stations 5, 6, 7) below 60°N, b) the northern stations (stations 1, 2, 3, 4) above 60°N situated where the Ob and the Irtysh rivers meet and along the Lower Ob River.

[40] Figures 4b and 4c shows the scatterplots of the snowmelt date versus the inundated extent in April (−0.86) and in May (0.88) for the southern stations for the period 1993-1996. In this case, the p-value equals 0.01 above a correlation of 0.708. The linear correlation coefficients are highly significant for both months. Figure 4b shows high values of the inundated extent in April when the

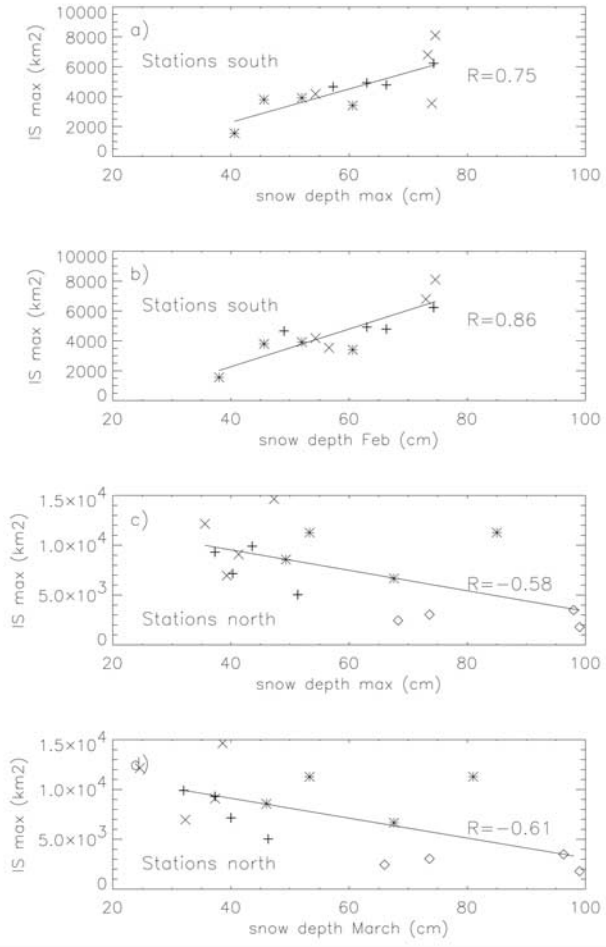


**Figure 5.** Scatterplot and linear regression results of the in situ snow depth observations and the satellite-derived inundated surfaces calculated over a 1° × 1° area centered on each station during the 1993–1996 period (a) the snow depth at maximum versus the inundated surfaces at maximum for the southern stations (station 5 with +, 6 with * and 7 with x) (b) the snow depth in February versus the inundated surfaces at maximum for the southern stations (c) the snow depth at maximum versus the inundated surfaces at maximum for the northern stations (station 1 with +, 2 with *, 3 with <> and 4 with x) (d) the snow depth in March versus the inundated surfaces at maximum for the southern stations.

snowmelt occurs in March and no flooding in April when the melting snow occurs in late April or May. The May inundation extent is very well correlated with the snowmelt date (Figure 4c) with the 0.99% confidence interval ranging from 0.62 to 0.96. The water released by the snowpack after melting from mid-April to late May produces a sharp increase in the inundated extent in May around the southern stations. However, the high values of inundated extent do not last more than a month since the floodwater drains into the hydrographic network of the Irtysh.

[41] Smaller correlations (P = 0.05 for correlation coefficients above 0.497) were found for the northern stations between the snowmelt date and the inundated extent in June (0.32) and July (0.41). However, Figures 4c and 4d clearly show a strong correspondence between the normalized snowmelt date and the normalized inundated extent in June and July (normalized means that the multiyear average is subtracted and the results divided by the standard deviation over the period). The respective linear correlations are highly significant with R = 0.89 for June and R = 0.93 for July. This suggests that the inundation extent at these northern sites are driven not only by local melting of snow but also by water coming downstream from the upper part of the basin.

[42] Figure 5 shows the scatterplots of the satellite-derived inundation at maximum extent versus the in situ snow depth observations. For the southern stations during 1993–1996, Figures 5a and 5b show a significant correlation and a good relationship between the inundated maximum extent and the maximum snow depth (0.75) and the snow depth in February (0.86, with the 95% confidence interval for 12 points ranging from 0.57 to 0.96). At these stations, a deeper snowpack during the winter produces a larger flooding extent. The difference in results observed between the snow depths at maximum and the snow depths in February can be explained by changes in the snow density during the winter. At this time, no data on the snow density evolution at the snow stations are available so this possibility could not be further investigated. However, we can conclude that over the southern stations, there is a close relationship between the winter snow depth and the satellite-derived maximum inundation extent in spring.

[43] No such relation was found for the northern stations. The associated correlations coefficients are negative and not significant. Figures 5c and 5d shows that the maximum inundated extent is not linked with the snow depth at maximum or the snow depth in March. For instance, station 3 (<>) is associated with approximately the same low inundated extent (3000 $km^2$) for large variations in the maximum snowpack depth (66 to 99 cm). Station 2 receives a small amount of snow each year (see Table 1) but the inundated extent around the station is large with large variations (from 7000 to 15000 $km^2$).

[44] For the northern stations, located closer to the main river channels, the water released locally from the snowpack is not the only contributor to the yearly maximum extent of inundation. In the case of locations connected with the large hydrographic network of the Middle Ob-Irtysh and the Lower Ob and fed by the large upstream basin, the flooding is also driven by the overall basin hydrology and water amount draining from the upstream basin. Moreover, river ice thickness can reach up to 2 m in normal winters over the northern Siberian coastal regions [*Vuglinsky*, 2002]. The delay of river ice breakup from south to north in this northern-flowing river allows the lower Ob basin to receive upstream runoff contribution and store the flow in the main river valley, resulting in the observed widespread flooding in the northern part of the basin.

[45] For the northern stations, we performed a multivariate correlation analysis to investigate the dependence of inundation maximum extent on both the snow depth at the station and the inundated extent in the upper basin. For station 2, we use the snow depth at maximum at the station and the sum of the maximum inundated areas for stations 3, 4, 5, 6, and 7. The linear correlation coefficient between

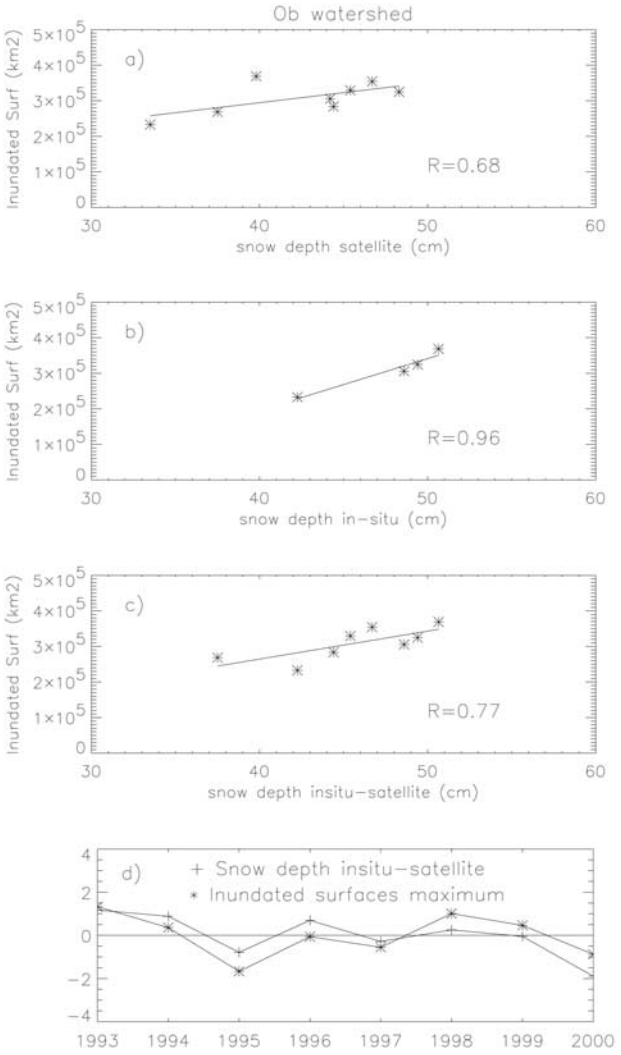


**Figure 6.** Ob basin-wide (52N–68N/61E–91E) results: (a) the total of inundated surfaces extent at maximum versus the spatially averaged snow depth in February derived from satellite observations for 1993–2000 (b) the total of inundated surfaces extent at maximum versus the spatially averaged snow depth in February from in situ observations for 1993–1996 (c) the total of inundated surfaces extent at maximum versus the spatially averaged combination over satellite-derived and in situ snow depth for 1993–2000 (d) the normalized anomalies of the inundated surfaces at maximum and the snow depth from in situ/satellite estimates.

snow depth at maximum and the inundated extent at maximum at station 2 is 0.20; the linear correlation coefficient between the inundated extents at maximum at station 2 and the sum of inundated extent at maximum for the stations in the upper basin is 0.8; the multivariate correlation gives a result of 0.95. Similar results were obtained for station 4, 3, and 1.

[46] Other factors may be considered to explain local variations of the inundated extent. The local topography of the area around the stations may also affect the inundated extent by increasing the water level rather than the extent. This should be checked more carefully in further studies by using measurements of the water level evolution derived from radar altimeter [*Frappart et al.*, 2005].

### 4.2. Basin-Wide Study Using Satellite Derived and In Situ Snow Data Set

[47] Another way to check the consistency of the inundation data set is to look at the basin-wide water balance measurements. Over a remote area such as the Ob basin, only remote sensing techniques offer a means to obtain information on the snow and flooding at basin scale. In this section, we consider the SSMI/I satellite-derived winter snow depths in February, spatially averaged over the Ob River Basin, for each year between 1993 and 2000 [*Grippa et al.*, 2005]. February was chosen by *Grippa et al.* [2005] as the most representative month for the winter snow depth over the Ob basin. The spatially averaged SSM/I snow depth in February for 1993–2000 has a mean value of 42.50 cm with a maximum of ~20 cm of variability. For the inundation data set, we consider the yearly maximum of the inundated extent over the Ob River Basin as presented on Figure 2.

[48] Figure 6a shows that the yearly maximum extent of inundation is significantly correlated (R = 0.68, p-value equals 0.05 above a correlation of 0.632) with the satellite-derived basin-wide snow depth in February for 1993–2000. This makes sense as a deeper snowpack basin-wide releases more water when melting and produces larger flooded areas.

[49] We also spatially averaged the in situ snow depth observations from the seven stations to estimate basin-wide snow depth in February for each year of 1993 to 1996. These stations cover a large range of latitudes within the basin so they might be representative of the entire basin. Figure 6b displays the yearly total extent of inundation with the in situ-derived basin-wide snow depth in February for 1993-1996. It shows a significant correlation (0.96) but a lower level of confidence (sample of 4).

[50] The results of the combination of satellite-derived snow depth and the in situ snow depth over the whole basin are presented on Figure 6c. For each year of 1993–1996, we obtained the in situ/satellite snow depth in February by calculating the mean of the satellite-derived snow depth and the basin-wide in situ snow depth observations. For 1997–2000, only the snow depth from satellite is available. There is a significant correlation coefficient (0.77, p-value equals 0.05 above a correlation of 0.632) that is higher than the one obtained on Figure 6a.

[51] In Figure 6d, the good relationship between the normalized inundation extent anomaly (difference between the yearly extents and the 8-year average divided by the 8-year standard deviation) and the normalized anomalies of the in situ/satellite snow depth estimates in February is shown. Years with less snow, as in 1995 and 1997, are associated with a negative anomaly in the basin-wide total inundated extent later in spring.

## 5. Flooding and Local River Runoff/Discharge Relations

[52] The inundation extent variations are compared systematically with the in situ runoff observations measured at

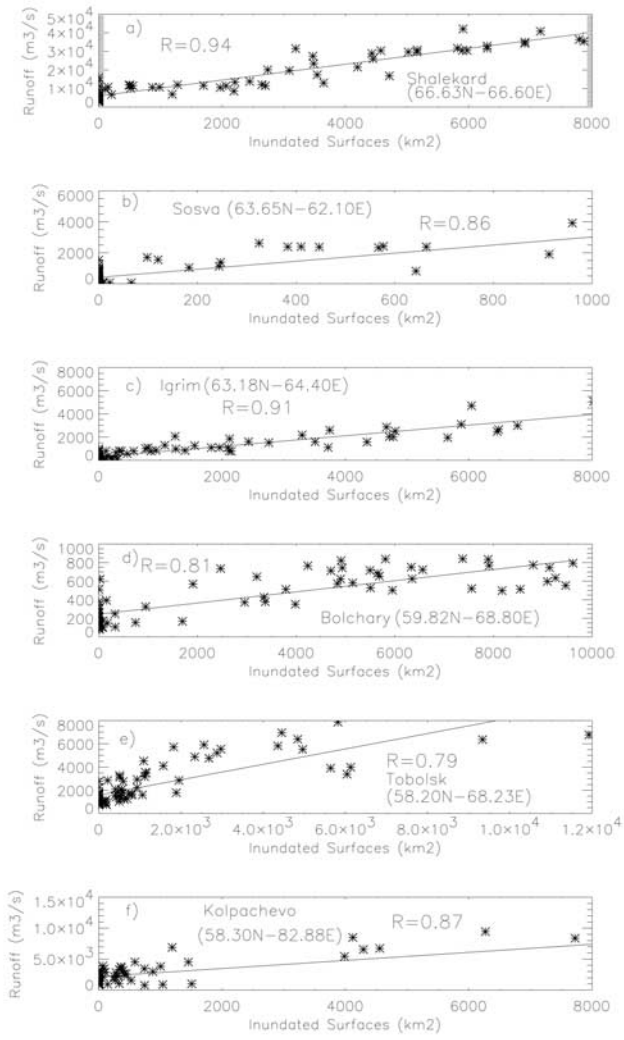


**Figure 7.** Scatterplot and linear regression results of the in situ runoff observations and the satellite-derived inundated surfaces for 6 locations. The inundation extents are calculated over a 1 × 1 degree area centered on the in situ runoff station (see Figure 1).

six different stations (see Figure 1 and Table 2) located over the Ob basin. Figure 7 displays the scatterplots and the associated linear regressions between the monthly inundated extent and the monthly in situ runoff for the six locations (96 points (8 years of monthly data) for station A (y = 4.27x + 604), 84 points for the stations B (y = 2.61 × + 406), C (y = 0.46x + 282), E (y = 0.06x + 244), 72 points for station D (y = 0.66 × + 1581) and 60 points for stations E (y = 0.65x + 2178)). These stations are representative of a large variety of river bodies over the basin, from small to large rivers as summarized on Table 2. The flooding extent estimates are averaged on 1 × 1 degree around the station where the in situ runoff is measured.

[53] The linear correlation coefficients obtained are very high. For station A, the correlation coefficient is 0.94 with the 99% confidence interval for 96 points ranging from 0.900 to 0.964. For all the locations, regardless of the characteristics of the streams, the runoff and the inundated extent are closely linked. Moreover, considering the topography, we found that the slope of the linear regression between the monthly flooding extent and the monthly runoff is highly correlated with the standard deviation of the topography (Table 2) for each location with R = 0.99. The sense of this relation is that larger topographic relief is associated with the more runoff for the same inundation extent.

[54] Figure 8 displays the normalized time series of satellite-derived inundation extent and the in situ runoff measurements of over five stations (station *F* is excluded in this analysis because the observations for 1995–1996 are not available). A strong correspondence is exhibited between the two data sets in their seasonal cycles. Regardless of the size of the stream, the seasonal and inter-annual variations of the two time series agree exceptionally well.

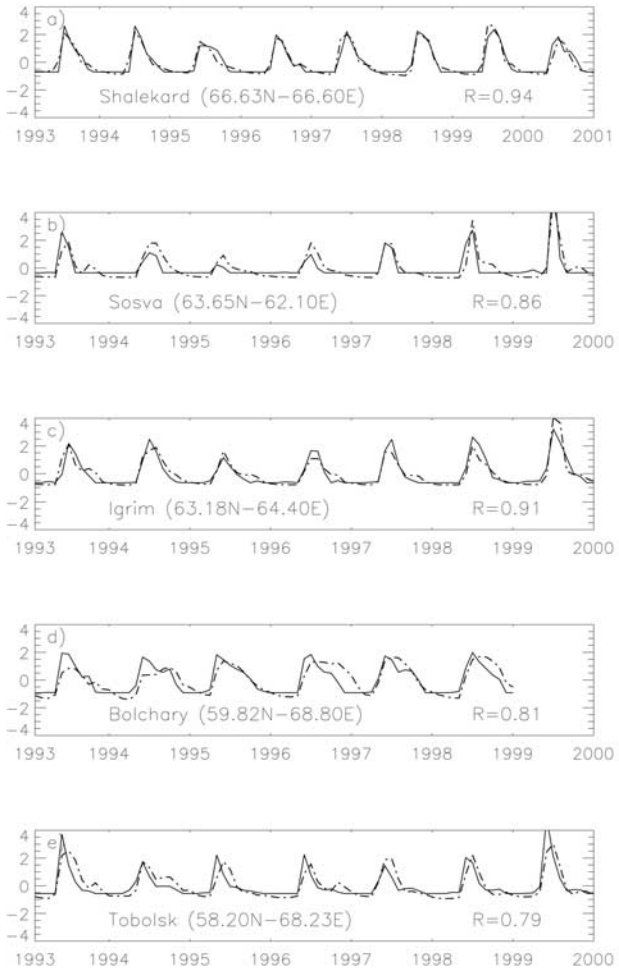


**Figure 8.** Comparison of the time series of the satellite-derived inundation extent and the in situ runoff measurements (dashed line) for five locations (for station A, B, C, D and E, see Figure 1). The inundation extent is calculated over a 1 × 1 degree area centered on station. Both variables are normalized (the mean is subtracted and the resulting values are divided by the standard deviation over the period).

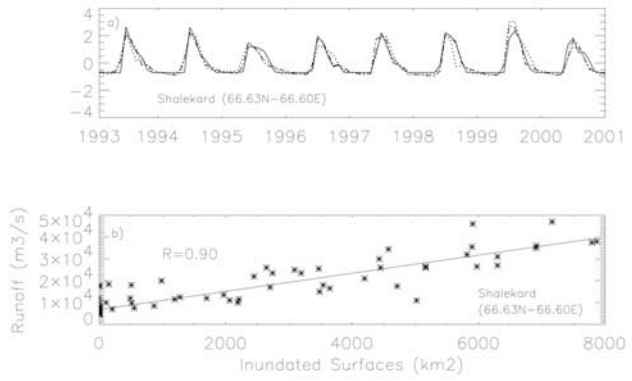


**Figure 9.** (a) comparison of the time series of the satellite-derived inundation extent and the satellite-derived discharge estimates (dotted line) over the Shalekard station. The in situ runoff at Shalekard station is also shown (dashed line). The inundation extent is calculated over a 1 × 1 degree area centered on station. Both variables are normalized (the mean is subtracted and the resulting values are divided by the standard deviation over the period); (b) Scatterplot and linear regression results of the satellite-derived inundation extent and the satellite-derived discharge estimates.

For the station Shalekard (station A), the peaks in the 1993 and 1994 in situ runoff are well captured by the inundation estimates. The peak in 1999 is less well reproduced at the beginning of spring. For the station B, the peaks in 1998 and 1999 are well captured, whereas for station C, the peak in the inundated extent is lower than the runoff. The opposite is observed for station E, where the peaks in the inundated extent for 1993 and 1999 are higher than for the runoff. For stations D and E, one can see a quasi-systematic lag-time of 1 or 2 months at the beginning of the increase and the yearly maximum between the inundated extent and the runoff. This can be related to the relationship between the inundated extent and the snowpack. Stations D and E are located in the same region as the "southern snow stations" of the section IVa. In this region, the inundated extents were found to be well correlated with the snowmelt date and the snow depth. When the snowmelt starts, the snowpack releases water that causes flooding. The excess water is then processed through the land and smaller streams before feeding the river itself.

[55] For the other stations A, B, and C situated further north, along rivers in the lower basin, there is almost no lag time observed between the inundated extent and the runoff observations. At Shalekard, the increase in runoff is even a bit earlier (1 month) that the increase in the inundated extent. These observations suggest that in this part of the basin, the inundated extent is due, in part to the local snow characteristics, but mainly to the water coming from the upstream basin and southern areas [*Yang et al.*, 2002]. The water released by the snowpack in the upper basin is drained and propagates northward through the large river network and contributes to the floods in the Lower Ob.

[56] Figure 9 shows another comparison between the inundated extent and another independent source of river discharge derived from satellite altimeter river-level measurements [*Kouraev et al.*, 2005]. This comparison shows really good agreement in the seasonal and inter-annual variations of the two normalized time series. The linear correlation between the two estimates is highly significant at 0.90 (p-value equals 0.01 above a correlation of 0.26. The high peaks that occur in 1993 and 1994 are well depicted. However, the peak in 1999 shows a difference in both estimates. As already observed on Figure 8a for the in situ runoff, there is a systematic time-lag of one month between the increase in the altimeter runoff estimate and the increase in the inundation extent. When the maximum in runoff is reached, the inundation extent variations agree better than the altimeter with the in situ runoff. The altimeter-derived discharge and the satellite-derived inundation are not in good agreement after the maximum in runoff is reached. However, after the seasonal peak in runoff is reached, the inundation extents still agree well with the in situ runoff. These observations highlight the complementarities of the two satellite techniques and the possible synergy of the satellite-derived inundated surfaces with the altimeter-derived water level measurements to provide a more accurate remotely sensed estimate of river runoff.

## 6. Conclusion

[57] This study reports a first effort to quantify and evaluate seasonality and extent of inundation using a suite of satellites over a boreal region, the Ob river basin. The multisatellite method that provides monthly inundation extent at global scale has been evaluated for tropical and-subtropical environments but the new data set still needed to be carefully evaluated in other regions like northern latitudes.

[58] In this paper, the seasonal and interannual variations of the monthly multisatellite-derived inundation extent over the Ob river basin have been evaluated by comparison to different independent proxies over the period 1993–2000. First, the consistency of the flooding variations is checked against variations of snowmelt date and snowpack depth, coming from in situ observations or derived from remote sensing passive microwave measurements. Second, the monthly inundation extent variations are compared to the variations of independent river runoff and discharge parameters from in situ observations and satellite altimeter-derived estimates. Over the four years of overlapping data available, a significant correlation is found between the in situ snow parameters and the inundation extent for the stations located in the southern region of the Ob river basin. Over these southern areas, the period of the satellite-derived maximum flooding extent is well correlated with the in situ snowmelt date. There is also a close relationship between the winter snow depth and the spring satellite-derived maximum inundation extent. For the northern stations, no such relations was found, as the water released locally from the snowpack is not the only contributor to the yearly maximum extent of inundation. Within the large hydrographic network of the Middle Ob-Irtysh and the Lower Ob, the flooding also depends on the water amount draining from the whole basin. A relationship between southern and northern inundation was demonstrated. At the basin-scale, the inundation data set was also found to be consistent with the SSM/I satellite-derived winter snow depths in February spatially

averaged over the Ob River. A good relationship was also found between the inundation extent and the river runoff and discharge estimated from in situ observations or satellite-derived measurements. The comparison shows really good agreement in the seasonal and inter-annual variations of the inundation extent and the river discharges.

[59] These results allow a cross-validation of the multi-satellite derived inundation, snow and river discharge data sets and strongly encourages the use of the remote sensing technique to monitor flooding events in boreal regions. Monitoring the flooding variability in the Northern river basin is fundamental to estimate the variability of freshwater flux to the Artic Ocean. A synergy with the radar altimeter water level estimates is under investigation. Combining the extent of floods from the multisatellite estimates with water level estimations from radar altimeters (Topex-Poseidon, ERS) will give information on surface water volume change over the Ob river basin, a crucial parameter for the biochemical and the hydrological cycles. Moreover, as the inundation data set is global, it can be used to analyze other large rivers basin in the Artic region such as the Lena or the Yenisey rivers, including other factors such as the permafrost effects in the flooding variations. Finally, the analysis reported in this paper is a useful step to improve the description of the snow-inundation-runoff relations in hydrological model over boreal river basins. Further work has to be done to investigate the relationships found in this paper by extending the data set to a much larger time period (to present ) and on a shorter timescale, for example on a weekly or daily basis.

## References


Adler, R. F., G. J. Huffman, A. Chang, R. Ferraro, P. Xie, J. Janowiak, B. Rudolf, U. Schneider, S. Curtis, D. Bolvin, A. Gruber, J. Susskind, and P. Arkin (2003), The Version 2 Global Precipitation Climatology Project (GPCP) monthly precipitation analysis 1979–present, *J. Hydrometeorol.*, *4*, 1147–1167.

Armstrong, R. L., and M. J. Brodzik (2005), Northern Hemisphere EASE-Grid weekly snow cover and sea ice extent version 3, National Snow and Ice Data Center, Boulder, Colorado USA.

Bousquet, P., et al. (2006), Contribution of anthropogenic and natural sources to atmospheric methane variability, *Nature*, *443*, 439–443, doi:10.1038/nature05132.

Bowling, L. C., D. P. Lettenmaier, B. Nijssen, L. P. Graham, D. B. Clark, and M. El Maayar (2003), Simulation of high latitude hydrological processes in the TorneKalix basin: PILPS Phase 2 (e), Experiment description and summary intercomparisons, *Glob. Planet. Change*, *38*, 1–30.

Cao, Z., M. Wang, B. Proctor, G. Strong, R. Stewart, H. Ritchie, et al. (2002), On the physical process associated with water budget and discharge over the Mackenzie basin during 1994/95 water year, *Atmopshere-Ocean*, *40*(2), 125–143.

Dickinson, B., B. I. J. Yashayaev, B. Meincke, S. D. Turrell, and J. Holfort (2001), Rapid freshening of the deep North Atlantic Ocean over the past four decades, *Nature*, *416*, 832–837.

Frappart, F., F. Seyler, J. M. Martinez, J. G. Leon, and A. Cazenave (2005), Floodplain water storage in the Negro River basin estimated from microwave remote sensing of inundation area and water levels, *Remote Sens. Environ.*, *99*, 387–399.

Fung, L. L., and A. Cazenave (2001), *Satellite altimetry and earth science, A handbook of techniques and application*, Academic Press, London, UK.

Gennero, M. C., J. F. Cretaux, M. Berge NGuyen, C. Maheu, K. Do Minh, S. Calmant, and A. Cazenave (2005), Surface water monitoring by satellite altimetry, http:// legos.obs-mip.fr/soa/hydrologie/hydroweb/, Laboratoire d'Etudes en Geodesie et Oceanographie Spatiale, Toulouse, France.

Grippa, M., N. Mognard, and T. Le Toan (2005), Comparison between the interannual variability of snow parameters derived from SSM/I and the Ob river discharge, *Remote Sens. Environ.*, *93*, 35–44.

Grippa, M., N. Mognard, T. Le Toan, and E. G. Josberger (2004), Siberia snow depth climatology derived from SSM/I data using a combined dynamic and static algorithm, *Remote Sens. Environ.*, *93*, 30–41.

Houweling, S., T. Kamisnki, F. Dentefer, J. Lelieveld, and M. Heinmann (1999), Inverse modeling of methane sources and sinks using the adjoint of a global transport model, *J. Geophys. Res.-Atmospheres*, *104*, 26,137–26,160.

Josberger, E. G., and N. M. Mognard (2002), A passive microwave snow depth algorithm with a proxy for snow metamorphism, *Hydrol. Process.*, *16*(8), 1557–1568.

Kalnay, E., M. Kanamitsu, R. Kistler, et al. (1996), The NCEP/NCAR 40-year reanalysis project, *Bull. Am. Meteorol. Soc.*, *77*, 437–470.

Kouraev, A. V., E. A. Zakharova, O. Samain, N. M. Mognard, and A. Cazennave (2005), Ob' River discharge from Topex-Poseidon satellite altimetry (1992-2002), *Remote Sens. Environ.*, *93*, 238–245.

Krenke, A. (2004), Former Soviet Union hydrological snow surveys, 1966–1996, National Snow and Ice Data Center/World Data Center for Glaciology, Boulder, Colorado, USA.

Matthews, E. (2000), *Wetlands in Atmospheric methane: its role in the global environment*, edited by M. A. K. Khalil, p. 202–233, Springer-Verlag, New York.

Matthews, E., and I. Fung (1987), Methane emission from natural wetlands: Global distribution, area, and environmental characteristics of sources, *Global Biogeochem. Cycles*, *1*, 61–86.

Mialon, A., A. Royer, and M. Fily (2005), Wetland seasonal dynamics and interannual variability over northern high latitudes derived from microwave satellite data, *J. Geophys. Res.*, *110*, D17102, doi:10.1029/2004JD005697.

Papa, F., C. Prigent, W. B. Rossow, B. Legresy, and F. Remy (2006a), Inundated wetland dynamics over boreal regions from remote sensing: The use of Topex-Poseidon dual-frequency radar altimeter observations, *Int. J. Remote Sens.*, *27*, 4847–4866, doi:10.1080/01431160600675887.

Papa, F., C. Prigent, F. Durand, and W. B. Rossow (2006b), Wetland dynamics using a suite of satellite observations: A case study of application and evaluation for the Indian Subcontinent, *Geophys. Res. Lett.*, *33*, L08401, doi:10.1029/2006GL025767.

Peterson, B. J., R. M. Holmes, J. W. McClelland, C. J. Vorosmarty, R. B. Lammers, and A. I. Shiklomanov (2002), Increasing river discharge to the Artic Ocean, *Science*, *298*, 2171–2173.

Prigent, C., E. Matthews, F. Aires, and W. B. Rossow (2001a), Remote sensing of global wetland dynamics with multiple satellite data sets, *Geophys. Res. Lett.*, *28*, 4631–4634.

Prigent, C., F. Aires, W. B. Rossow, and E. Matthews (2001b), Joint characterization of vegetation by satellite observations from visible to microwave wavelength: A sensitivity analysis, *J. Geophys. Res.*, *106*, 20,665–20,685.

Prigent, C., F. Papa, F. Aires, W. B. Rossow, and E. Matthews (2007), Global inundation dynamics inferred from multiple satellite observations, 1993–2000, *J. Geophys. Res.*, D12107, doi:10.1029/2006JD007847.

R-ArcticNet v 2.0 (2003), A regional, electronic, hydrographic data network for the Arctic region, http://www.r-arcticnet.sr.unh.edu/.

Rossow, W. B., and R. A. Schiffer (1999), Advances in understanding clouds from ISCCP, *Bull. Am. Meteorol. Soc.*, *80*, 2261–2287.

Smith, L. C. (1997), Satellite remote sensing of river inundation area, stage and processes: A review, *Hydrol. Process.*, *11*, 1427–1439.

Vuglinsky, V. S. (2002), Particularities of ice events in Russian Arctic rivers, *Hydrol. Process.*, *16*, 905–913.

Walter, B., M. Heinmann, and E. Matthews (2001), Modeling modern methane emission from natural wetlands. 1. Model description and results, *J. Geophys. Res.*, *106*(D24), 34,189–34,206.

Yang, D., D. Robinson, Y. Zhao, T. Estilow, and B. Ye (2003), Stream flow response to seasonal snow cover extent changes in large Siberian watersheds, *J. Geophys. Res.*, *108*(D18), 4578, doi:10.1029/2002JD003149.

Yang, D., D. L. Kane, L. D. Hinzman, X. Zhang, T. Zhang, and H. Ye (2002), Siberian Lena river hydrologic regime and recent change, *J. Geophys. Res.*, *107*(D23), 4694, doi:10.1029/2002JD003149.

Zhang, T., R. G. Barrr, K. Knowles, J. A. Heginbottom, and J. Brown (1999), Statistics and characteristics of permafrost and ground-ice distribution in the Northern Hemisphere, *Polar Geog.*, *23*, 132–154.



F. Papa, NASA-Goddard Institute for Space Studies-Columbia University, 2880 Broadway, New York, NY 10025, USA. (fpapa@giss.nasa.gov)

C. Prigent, CNRS, Laboratoire d'Etudes du Rayonnement et de la Matiere en Astrophysique, Observatoire de Paris, France.

W. B. Rossow, NOAA-Cooperative Remote Sensing Science and Technology Center, City College of New York, NY, USA.